Laser Peening Effects on High-Cycle Fatigue Properties of Al-Li Friction Stir Welded Joints: Crystal Plasticity Modeling & Quantitative Evaluation

Maziar Toursangsaraki and Yongxiang Hu*

State Key Laboratory of Mechanical System and Vibration, School of Mechanical Engineering, Shanghai Jiao Tong University, Shanghai, China

Abstract
To optimize surface treatment procedures, their strengthening mechanisms need to be evaluated on the material properties. In this study, physics-based relations were employed with crystal plasticity constitutive equations to quantify the strengthening effects of microstructural attributes on the high-cycle fatigue properties of the AA2195-T6 friction stir welded joints after applying multiple laser peening layers. The developed model quantified the contributions of laser-peening-induced near-surface compressive residual stresses, dislocation density increase, and crystal morphology variations on the evolutions in fatigue indicator parameters. Grain-average fatigue indicator parameters were utilized to evaluate the fatigue property modification trends with depth, while their extreme values estimated the corresponding improvements at grain boundaries in near-surface regions after laser peening. As the crystal plasticity model predicted, the enhancement in joint fatigue properties mainly stemmed from the alleviation of cyclic mean stress under near-surface compressive residual stresses. This effect was followed by the increased resistance to cyclic plastic deformation due to the rise in dislocation density and texture intensity, and the decrease in crystal morphology heterogeneity under the homogenization of crystal morphology after laser peening. The decrease in extreme-value and grain-average fatigue indicator parameters in depth were the mechanisms behind enhancements in joint surface fatigue properties and the relocation of fatigue failure regions from surface to subsurface areas. Moreover, experimental high-cycle fatigue observations revealed the improvement in joint fatigue properties and validated the numerical approaches.
Keywords: Crystal plasticity, Laser peening, Friction stir welding.

Introduction

Friction stir welding (FSW) has been proven beneficial for joining Al-Li alloys owing to the superior joint properties compared to conventional fusion welding processes. However, its major limitation is the relative strength reduction at the joint center under the dissolution of precipitate phases and crystal texture alleviation caused by the thermo-mechanical procedures during welding. Hence, modification processes are necessary to regain the degraded joint mechanical properties. Laser peening (LP) has been extensively utilized to improve the fatigue properties of Al FSW joints. This process induces deeper near-surface plastic deformation, compressive residual stresses, and lower surface damage among mechanical surface treatment methods [1]. The LP-induced enhancements in material fatigue properties have been attributed to compressive residual stresses, work-hardening, and texture variations in near-surface regions under LP [2]. Microstructure-sensitive modeling techniques are necessary to quantify the strengthening contributions of LP effects on improving the joint fatigue properties.

The crystal plasticity (CP) modeling method simulates the crystal lattice and slip formation as the source of elastic-plastic deformation behavior. CP finite element method (CPFEM) includes the microstructural attributes of polycrystals in the CP constitutive modeling. Toursangsaraki et al. conducted the Eigenstrain technique on the CPFEM framework to predict the LP-induced residual stress distribution under texture anisotropy of A2024-T31 sheets [3]. Stopka et al. employed the fatigue indicator parameter (FIP) developed by

Fatemi-Socie to include the slip plastic shear strain and slip normal stress as the mechanisms behind high-cycle fatigue (HCF) crack initiation for AA7075-T6 [4].
Physics-based CPFEM models have been developed to quantify the strengthening effects of microstructural attributes, including grain size, crystal morphologies, dislocation density, deformation twinning, and precipitate phases, in material deformation mechanisms. Toursangsaraki et al. developed local physics-based CPRVE LP models at central regions of Al-Li FSW joints to quantify the LP strengthening effects on enhancing the joint tensile properties, including compressive residual stresses, and dislocation density elevation, and crystallographic texture intensification [5]. There has yet not been a material modeling approach to quantify the LP strengthening contributions to modifying HCF properties.
This study developed the physics-based CPFEM fatigue model of AA2195-T6 FSW joints to investigate the modification mechanisms in their fatigue properties under the application of multiple LP layers. This model quantified the contributions of LP effects on the variations in the distribution of FIPs, including compressive residual stresses, dislocation density increase, and crystal morphology alterations in near-surface regions. Experimental HCF tests were conducted on FSW joints at different LP conditions to observe the improvements in the joint fatigue properties under LP and validate the modeling outputs.

Experimental Methods
Rolled sheets of AA2195-T6 were FSWed in a butt-joint application. FSW joints generally show three relatively discrete zones, including the stirring zone (SZ), thermo-mechanically affected zone (TMAZ), and heat-affected zone (HAZ). An H13 tool with an 18 mm shoulder diameter and 6 mm threaded-pin diameter was employed using a normal force of 6 kN and tilt angle of 1°. The tool rotational and welding speeds were set at 270 mm/min and 500 RPM, respectively.
Double-sided LP was applied at the joint center to modify the joint fatigue properties. Specimens were fixed on an industrial robot arm that moved it in the LP direction with16 mm/s constant velocity to impose a uniform pattern of LP with the overlap ratio of 20% at each two successive shock impacts. An Nd: YAG laser beam with the wavelength of 1064 nm, power density of 10 J, the repetition frequency of 5 Hz, and duration of 15 ns was applied, which induced circular 4mm diameter impact spots on the surface.
Stress-controlled HCF tests were employed with a maximum nominal stress of 200 MPa, a ratio of 0.1, and a frequency of 15 Hz to reveal the LP effects on the joint fatigue life and failure mechanisms.

Modeling process
Because fatigue failure happened at SZ in all LP conditions, CPRVEs were only developed at this zone to evaluate LP modifications on the HCF properties of FSW joints. LP effects were measured by experiments after each LP layer and inserted into the CPRVE of SZ to quantify their contributions to the strengthening mechanisms under LP. This study utilized the previously measured LP-induced near-surface residual stresses, dislocation density, and crystal texture variations for similar FSW joints in the reference [5]. This study used the Eigenstrain distribution data calculated in the reference [5] to match the simulated LP-induced residual stress distribution with depth in the SZ CPRVE with the experimentally measured values by the X-ray diffraction (XRD) application. Then, the XRD measured distribution of dislocation density values was inserted to its corresponding CPRVE depth. Near-surface crystal orientation distributions were obtained by the electron backscattered diffraction (EBSD) process after each LP layer and synthesized into the CPRVE at SZ in its corresponding depth after each LP layer.
CP constitutive equations resolve the Cauchy stress to the crystal slip system α by multiplying its components with the dyadic product of the slip direction and normal plane unit vectors to calculate the slip shear stress. The cumulative deformation gradient is described by the multiplicative decomposition of rigid body rotation of crystal lattice and crystal slip deformation to represent the microscopic elastic/plastic deformation [6]. The physics-based CP model considers the slip strengthening effects of the various material microstructural

features, including grain size, crystal morphologies, and dislocation density. The critical resolved shear stress $\tau_{\mathrm{cr}}^{\alpha}$ of each slip system has been obtained as the cumulative effects of intrinsic crystal slip strength of Al alloys (τ_0^{α}), dislocation density effects ($\Delta\tau_{\mathrm{dis}}^{\alpha}$), and grain size strengthening ($\Delta\tau_{\mathrm{HP}}^{\alpha}$) by [5]

$$\tau_{\mathrm{cr}}^{\alpha} = \tau_0^{\alpha} + \Delta\tau_{\mathrm{HP}}^{\alpha} + \Delta\tau_{\mathrm{dis}}^{\alpha} \tag{1}$$

The Hall-Petch relation has empirically predicted the strengthening effects of Grain-size on the crystal slip strength as

$$\Delta\tau_{\mathrm{HP}}^{\alpha} = \frac{K_0}{\sqrt{D_G}} \tag{2}$$

with $K_0 = 0.06\,\mathrm{MPa}\sqrt{\mathrm{m}}$ being the Hall-Petch constant for Al alloys, and D_{G} defining the grain size average value. The dislocation density effects on the slip strength have been obtained by

$$\Delta\tau_{\mathrm{dis}}^{\alpha} = \mu G b\sqrt{\rho} \tag{3}$$

with G being the Al matrix shear modulus, b describing the Burger's vector of the gliding dislocations, μ=0.2 defining the calibrated slip interactions for the Al matrix, and ρ as the total dislocation density, which is the summation of dislocation density values at different slip systems. The dislocation density evolutions under plastic deformation have been related to the grain size and current value of dislocation density value by

$$\dot{\rho}^{\alpha} = \left(\frac{C}{D_G} + K_a\sqrt{\sum_{\beta=1}^{n}\rho^{\beta}} - k_b\rho^{\alpha} \right)\left|\dot{\gamma}^{\alpha}\right| \tag{4}$$

where C is a grain size effect constant, and k_a and k_b include the generation and annihilation phenomenon of dislocation density, respectively. The UMAT subroutine is employed to insert the physics-based CP constitutive equations into the ABAQUS solver.

Fatemi and Socie FIP considers the critical plane where the highest maximum normal stress and cyclic plastic shear strain range occur. By considering the crystal slip as the source of plastic deformation, this FIP relation has been presented for slip planes by [4]

$$P_{\mathrm{FS}} = \frac{\Delta\gamma_{\mathrm{p,max}}^{\alpha}}{2}\left(1 + k_{FS}\frac{\sigma_{\mathrm{n,max}}^{\alpha}}{\sigma_0}\right) \tag{5}$$

with $\Delta\gamma_{\mathrm{p,max}}^{\alpha}$ describing the maximum cyclic plastic slip shear strain range on the slip plane, $\sigma_{\mathrm{n,max}}^{\alpha}$ as its normal stress, and σ_0 defining the material yield strength. The constant value of $k_{\mathrm{FS}} = 1$ characterizes the intensity of normal stress effects for the Al matrix.

The slip misorientations among neighboring grains cause the discontinuity of dislocation motions at the grain boundaries and the concentration of stress-strain values at these interfaces during material deformation. Moreover, crystallographic orientations define the grain strength by the material Taylor factor. The FCC crystal grains with the dominance of $\{110\}_{\mathrm{Al}}$ orientations are softer. On the other hand, the relative dominance of $\{111\}_{\mathrm{Al}}$ and $\{100\}_{\mathrm{Al}}$ texture components are induced under plastic deformation and increase the grain strength [7]. The localization of plastic deformation at the softer side of hard/soft grain boundaries is caused by the combined effect of crystallographic misorientation and mechanical property heterogeneity. Thus, the grain boundaries with relatively higher misorientation angles and the mechanical property differences are more sensitive for extreme-value FIPs and fatigue crack formation under HCF loading. FIP extreme value distributions have been fit to the Gumbel probability distribution function to statistically analyze their distributions by

$$p = \exp(-e^{-\alpha_n (y_n - u_n)}) \quad (6)$$

where $p = F_{Y_N}(y_n)$ defines the possibility of Y_N value being lower than or equal to y_n which is a member of the population. The factor of $u_n$describes the characteristic highest members of the extreme-value population. Hence, higher u_n amounts indicate larger maximum values occurring within the extreme-value population. The α_n value denotes an inverse measure of occurring dispersions around the most significant characteristic extreme values. Higher α_n shows Lower dispersion in maximum extreme values.

Joint mechanical properties were considered homogeneous in the welding direction. Thus, joint cross-section 2D plane-strain CPRVEs were sufficient to model its HCF properties. DREAM.3D instantiated the EBSD-obtained crystal texture into the ABAQUS software input file to generate joint local CPRVEs with CPE4R elements. Two types of CPRVE were developed for the HCF modeling at SZ. The surface CPRVE illustrated extreme-value FIP variations at near-surface grain boundaries. On the other hand, half-depth CPRVEs simulated LP-induced variation in grain-average FIPs with depth. The simulated HCF tests consisted of a displacement-controlled cyclic loading with the maximum mean stress value of 200 MPa and a ratio of 0.1 for both surface and half-depth CPRVEs corresponding to the HCF experiments. The current CPFEM fatigue model utilized the previously obtained physics-based CP parameters for similar FSW joints presented in the reference [5].

Results and discussions

This study utilized previously measured microstructural evolutions of similar FSW joints under LP of similar FSW joints to evaluate the joint HCF enhancement under multiple-LP [5]. The texture recrystallization at SZ under FSW thermo-mechanical effects generated the refined grain texture with high-angle grain boundary distribution. LP-induced surface plastic deformation relatively reduced the misorientation angles through homogenizing the crystal texture towards $\{111\}_{Al}$ component. Fig. 1 illustrates the contributions of multiple-LP effects on the Gumbel distributions of near-surface FIP extreme values at SZ. Each LP effect decreased near-surface FIPs contributing to the improvement in surface HCF properties.

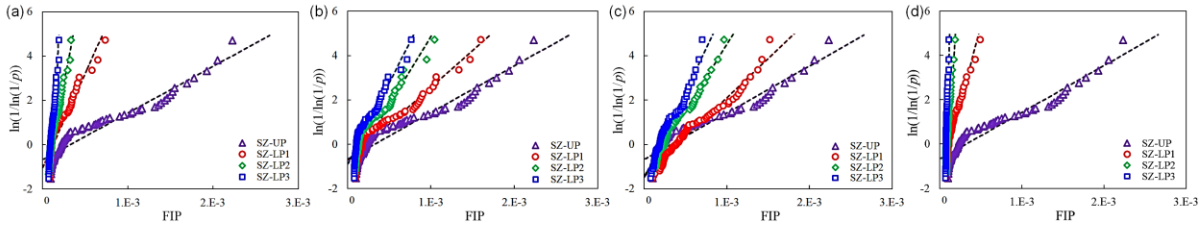

Fig. 1 Multiple-LP effects on the Gumbel distributions of surface extreme-value FIPs at SZ: (a) residual stresses; (b) dislocation density; (c) crystal morphologies; (d) combined effects.

Table 1 compares various contributions of LP effects on the FIP factors after the third layer of LP. α_n was most significantly affected by the compressive residual stresses at 74% of the combined LP effects, followed by crystal morphology variations at 15% and dislocation density evolutions at 11%. Corresponding LP contributions on u_n values was 59%, 21%, and 20%, respectively. This also showed a more noticeable improvement in the peak FIP extreme-value variations under texture modification than dislocation density.

Table 1 LP-induced variations in Gumbel distribution parameters of extreme-value FIPs.

LP effects	α_n /contribution %	u_n /contribution %
Unpeened	2e3	6.9e-4
Residual stresses	4.3e4 / 74%	1.2e-4 / 59%
Crystal morphology	8.3e3 / 15%	2.6e-4 / 21%
Dislocation density	7.2e3 / 11%	2.7e-4 / 20%
Total effects	7e4(270%↑)	9e-5(91%↓)

Table 2 compares various contributions of LP effects on the variations of grain-average FIPs with depth at SZ. Compressive residual stresses were the main contributors to the decrease in FIP values at about 62% of all contributions under all LP conditions, followed by dislocation density elevation at about 25% and crystal morphology variations at about 12%. Thus, compressive residual stresses led to the main HCF enhancement mechanism by reducing slip normal stress and cyclic plastic shear strain as crack formation mechanisms. Dislocation density elevation and Crystal morphology evolutions ranked second and third, respectively, in the joint fatigue property improvement in depth by increasing the material yield strength and resistance against slip cyclic plastic shear strain.

Table 2 Contributions of LP impacts in the variations of grain-average FIPs.

LP layers	RS / %	Dislocation / %	Texture / %	Total /Decrease %
Unpeened	5.9e-4/0	5.9e-4/0	5.9e-4/0	5.9e-4/0
LP1	1.5e-4 / 64%	3.2e-4 / 24%	4.1e-4 / 12%	9.7e-5/84%
LP2	1.02e-4/ 62%	2.1e-4 / 25%	3.1e-4/ 13%	4.2e-5/93%
LP3	8e-5 / 61%	1.6e-4 / 25%	2.6e-4/ 14%	3e-5/95%

Fig. 2 shows the grain-average FIP distributions at the slip planes for different LP conditions at SZ. FIPs kept reasonably constant values at around 5.9e-4 with depth before LP. Near-surface compressive residual stresses led to the highest effects on FIP values with depth, followed by dislocation density increase and crystal morphology variations. The highest FIP value alterations occurred at the first LP layer for all LP effects, and the corresponding evolutions decreased after each successive LP layer due to the saturation of near-surface plastic deformation and work-hardening under LP.

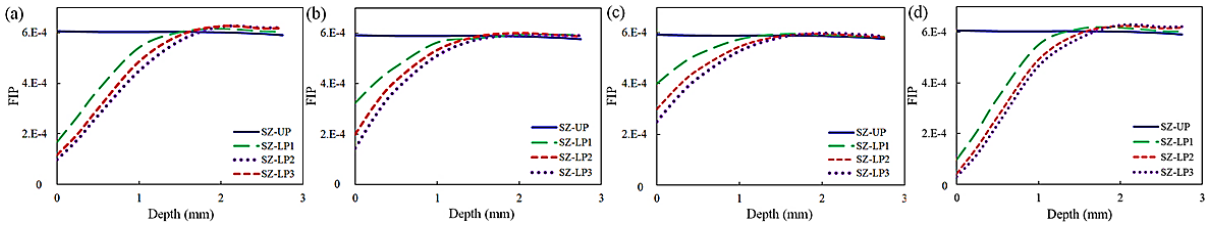

Fig. 2 Grain-average FIP values with depth under different multiple-LP effects at SZ: (a) Residual stresses; (b) Dislocation density; (c) Crystal morphology; (d) Combined effects.

Fig. 3a shows the experimental HCF results for the enhancement in HCF properties of AA2195-T6 and its FSW joints under multiple LP effects. Fig. 3b&c compare the joint fatigue fracture surfaces for the unpeened condition and third LP layer. The FCI for the unpeened condition occurred at the SZ surface because of lower fatigue resistance in the material surface and moved to the depth after LP, second, and third layers of LP because of the HCF resistance modification at surface-surface regions after LP. The in-depth FCI areas presented slightly less brittle failure mechanisms owing to the higher requirement for local accumulation of plastic deformation at these locations before failure [8].

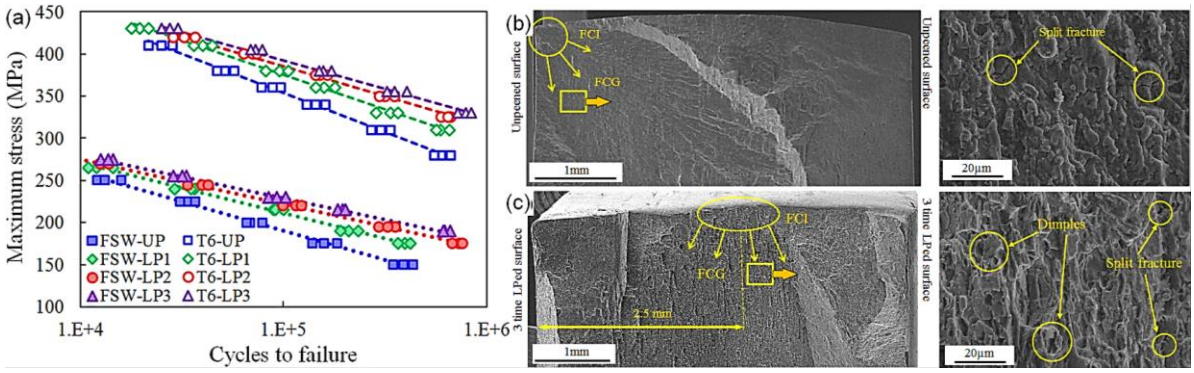

Fig. 3 HCF test results: (a) HCF life; failure surface for unpeened (b) and third LP layer (c).

Discussion and Conclusions

This study evaluated the mechanisms behind multiple-LP-induced modification in the HCF life of the AA2195-T6 FSW joints by developing the joint local physics-based CPFEM fatigue model at SZ. Overall conclusions were sorted as follows:

(1) The CPRVE fatigue model reasonably analyzed the LP modification mechanisms on the joint fatigue properties at SZ by quantifying various contributions of LP effects in reducing FIP values in this region.

(2) HCF strengthening features under LP were sorted as 1- cyclic mean stress reduction because of compressive residual stresses; 2- increase in resistance against cyclic microplastic deformation under the elevation of dislocation density and texture intensity; 3- the decrease in misorientations and heterogeneity of mechanical properties at grain boundaries under the texture homogenization effects.

(3) The most significant LP contributions in decreasing joint grain-average FIPs at SZ stemmed from the near-surface compressive residual stresses, followed by dislocation density evolutions and crystal texture variations after LP. Under the grain-boundary misorientation reduction, the texture variations effects in reducing surface extreme-value FIPs were higher than dislocation density effects.

(4) HCF test results indicated the improvements in the joint fatigue life and failure mechanisms by relocating FCI regions from the surface areas to the depth under multiple-LP effects and validated the modeling results.

Acknowledgments

This work was supported by the National Natural Science Foundation of China (Grant number U21A20135), “Shuguang Program” of Shanghai Education Development Foundation, Shanghai Municipal Education Commission (Grant number 20SG12), and Shanghai R&D public service platform project (Grant number 19DZ2291400).

References

[1] R. Yang, Y. Hu, M. Luo, H. Cheng, Z. Yao, *Distortion control of thin sections by single-sided laser peening*, Optics and Lasers in Engineering, 115 (2019) 90-99.

[2] Y. Sano, K. Masaki, T. Gushi, T. Sano, *Improvement in fatigue performance of friction stir welded A6061-T6 aluminum alloy by laser peening without coating*, Materials & Design (1980-2015), 36 (2012) 809-814.

[3] M. Toursangsaraki, H. Wang, Y. Hu, D. Karthik, *Crystal Plasticity Modeling of Laser Peening Effects on Tensile and High Cycle Fatigue Properties of 2024-T351 Aluminum Alloy*, Journal of Manufacturing Science and Engineering, 143 (2021).

[4] K.S. Stopka, M. Yaghoobi, J.E. Allison, D.L. McDowell, *Effects of boundary conditions on microstructure-sensitive fatigue crystal plasticity analysis*, Integrating Materials and Manufacturing Innovation, 10 (2021) 393-412.

[5] M. Toursangsaraki, Y. Hu, T. Zhang, *Crystal plasticity quantification of laser peening strengthening effects on AA2195-T6 friction stir welded joints*, The International Journal of Advanced Manufacturing Technology, (2022) 1-21.

[6] W.D. Musinski, D.L. McDowell, *On the eigenstrain application of shot-peened residual stresses within a crystal plasticity framework: Application to Ni-base superalloy specimens*, International Journal of Mechanical Sciences, 100 (2015) 195-208.

[7] W. Liu, H. Huang, J. Tang, *FEM simulation of void coalescence in FCC crystals*, Computational Materials Science, 50 (2010) 411-418.

[8] S. Farfan, C. Rubio-Gonzalez, T. Cervantes-Hernandez, G. *Mesmacque, High cycle fatigue, low cycle fatigue and failure modes of a carburized steel*, International Journal of Fatigue, 26 (2004) 673-678.